Infiltration of CNT forests by Atomic Layer Deposition for MEMS Applications

by

Collin Brown

A senior thesis submitted to the faculty of

Brigham Young University

in partial fulfillment of the requirements for the degree of

Bachelor of Science

Department of Physics and Astronomy

Brigham Young University

April 22, 2014

BRIGHAM YOUNG UNIVERSITY

DEPARTMENT APPROVAL

of a senior thesis submitted by

Collin Brown

This thesis has been reviewed by the research advisor, research coordinator, and department chair and has been found to be satisfactory.

Date	David D. Allred, Advisor
Date	Eric G. Hintz, Research Coordinator
Date	Richard Vanfleet, Chair

ABSTRACT

Infiltration of CNT forests by Atomic Layer Deposition for MEMS Applications

Collin Brown

Department of Physics and Astronomy

Bachelor of Science

The fabrication of microelectromechanical systems (MEMS) is generally limited by the same processes and materials used in the semiconductor industry. We have been investigating the infiltration of patterned carbon nanotube (CNT) forests to find more materials and potentially easier methods to make MEMS. Our goal is to fill in the void between the nanotubes in the CNT forest with deposited metal, creating a solid metal-carbon hybrid in the same shape as the CNT forest. Previous students here at BYU investigated the infiltration of molybdenum and tungsten metal using molybdenum carbonyl and tungsten carbonyl, respectively, as precursors in chemical vapor deposition (CVD). The current topic of research is infiltration by atomic layer deposition (ALD) using tungsten hexafluoride and hydrogen (including atomic hydrogen via microwave plasma) as precursors. In the course of this research, we have seen the tungsten deposited as a crust over the top of the CNT forest, penetrating only microns into the forest.

ACKNOWLEDGMENTS

I would like to thank my wonderful and beautiful wife for supporting me in my studies and research. I am very grateful for the Physics department, ORCA, and MEG grant funding that I recieved over the course of this research. Without it I wouldn't have been able to devote near as much time to the project. I am grateful to Professor David Allred for his continued guidance on the project, to Professor Richard Vanfleet for his direction, and to Professor R. Steven Turley for his help in writing and formatting this paper. I am also very grateful for the students in the various groups that have helped me in this project, including Kyle Anderson who worked on the project with me, Lawrence Barrett, Kenneth Hinton, Joseph Rowley and others. Without their help, this project would not have been possible.

Contents

Bibliography **26**

List of Figures

Chapter 1

Introduction

1.1 MEMS

Figure 1.1: A micromotor, one application of MEMS technology[1].

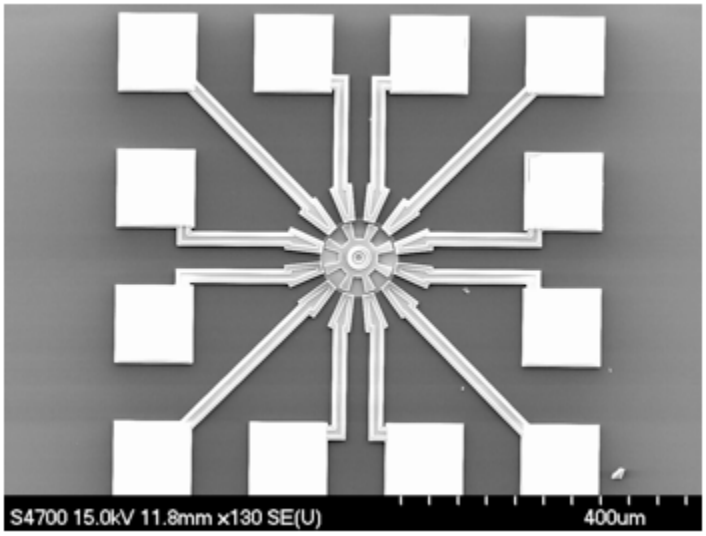

Microeletromechanical systems (MEMS) are used in many everyday applications. Most likely the most well-known application is the comb drive accelerometer found in game devices and most cell phones today. This accelerometer allows the phone to know how you move the phone, and

which way is down. Other MEMS applications include gyroscopes, inertial modules, digital compasses, microphones, humidity sensors and pressure sensors[5]. The micro system analyzers also known as "lab-on-a-chip" devices are also a MEMS application.

In order to increase the applications for MEMS, we have been researching the fabrication of MEMS out of refractory metals using non conventional methods. Conventional MEMS fabrication is achieved by patterning the sample through lithography, and then etching away portions of the sample that should be removed. This is a powerful method and has been used for most of the MEMS devices we see today. However, when the pattern desired is high-aspect-ratio structures, meaning very thin deep holes or trenches, etching runs into some problems. There exists a critical or maximum achievable aspect ratio with regard to etching[6]. When the etching gets very deep, the chemical reactant cannot get down to bottom of the trench, and each etch cycle takes progressively longer.

Many have studied how to take traditional etching methods and make them more effective for high-aspect-ratio structures. To solve this problem, we have chosen a different additive process, rather than a subtractive process like etching. We will build up a high-aspect-ratio MEMS structure using templated carbon nanotubes as a scaffold.

1.2 Carbon Nanotubes

The study of carbon nanotubes along with other forms of graphitic carbon has been a hot topic in the materials world since their introduction in 1991

Figure 1.2: Single wall nanotube with armchair configuration.[2]

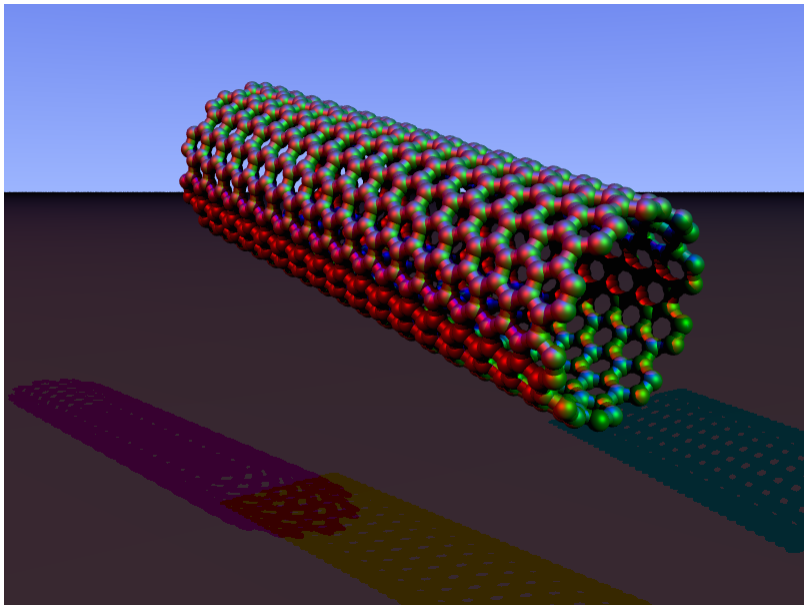

by Sumio Iijima[7]. Carbon nanotubes and graphene are very interesting due to their impressive electrical and mechanical properties. These nanotube structures are basically rolled up sheets of graphene, and thus have many similar properties with graphene.

Based on the different crystal structure of the nanotube, a carbon nanotube can either be a small band gap semiconductor or a conductor. Based on these properties, there are many efforts to incorporate carbon nanotubes into semiconductor devices. So far, researchers have succeeded in creating field effect transistors from carbon nanotubes[8]. For those nanotubes that have the structure to be conductors, these nanotubes can carry impressive current density. This current carrying capacity is also important in creating higher power semiconductor devices.

Thermal conductivity in nanotubes is interesting, as they are very good conductors along the tube, but across the tube they are insulators. In tests done from the 300-800 K range, carbon nanotubes displayed thermal conductivity of 3500 W/m.K at room temperature and decreasing similar to 1/T as temperature rose[9]. This is impressive, as the thermal conductivity of metals like copper is around 400 W/m.K.

Carbon nanotubes have impressive tensile strength, with certain tests yielding up to 63 gigapascals (GPa)[10]. However, this only pertains to single nanotubes under tensile stress. The nanotubes deform under compressive stress, bending, or torsional stress. For a nanotube forest, the tubes are held together by only weak van der walls forces, and templated nanotubes fall apart easily without something else to bind them together. Bringing the nanotubes together so that they form a coherent and strong structure is a very important aspect of our research.

Finally, at Brigham Young University, a process for creating vertically aligned carbon nanotube structures in a template was developed[11]. This process, called carbon nanotube templated microfabrication (CNT-M), allows us to use the low density carbon nanotube forest as a scaffold for deposition. The CNT-M process has been used successfully to fabricate MEMS from amorphous carbon (a-C), silicon, silicon dioxide (SiO_2), and silicon nitride (Si_3N_4), all built upon the scaffold of carbon nanotubes[11, 12]. This process allows us to make MEMS with a higher aspect ratio than those fabricated by traditional etching methods. This paper focuses on the infiltration of the forests with tungsten metal.

1.3 Theory of Atomic Layer Deposition (ALD)

$$2WF_{6\,(g)} + 3H_{2\,(g)} \Longrightarrow 2W_{(s)} + 6HF_{(g)} \tag{1.1}$$

Atomic layer deposition, hereafter referred to as ALD, is a powerful method for producing epitaxial single atom thin films. The theory behind ALD is that two or more precursor gases deposit or react with the substrate in sequential order. The first gas adheres to the substrate in a self limiting layer, meaning that the precursor molecules only adhere to the substrate and not to other precursors. The second gas then reacts with that layer, with part of the material leaving in the gas phase, and part of the material depositing. The figure below describes a 2 species atomic layer deposition process, but the theory is the same with as with 1 species in the layer.

Figure 1.3: Atomic layer deposition of a 2 species film. [3]

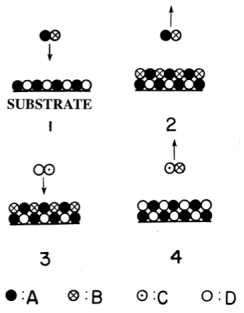

This process can be repeated many times to build up thick layers. Compared to chemical vapor deposition, there is more control at the cost of complexity and time. Of particular note to our system is the enthalpy of particular reactions. The tungsten ALD reaction is endothermic, and will take absorb heat in the process. Thus we would like the substrate

Figure 1.4: Test structures infiltrated with $W(CO)_6$. The micrograph on the right shows a infiltrated forest that has crumbled under the scratch test, indicating insufficient deposition.[4]

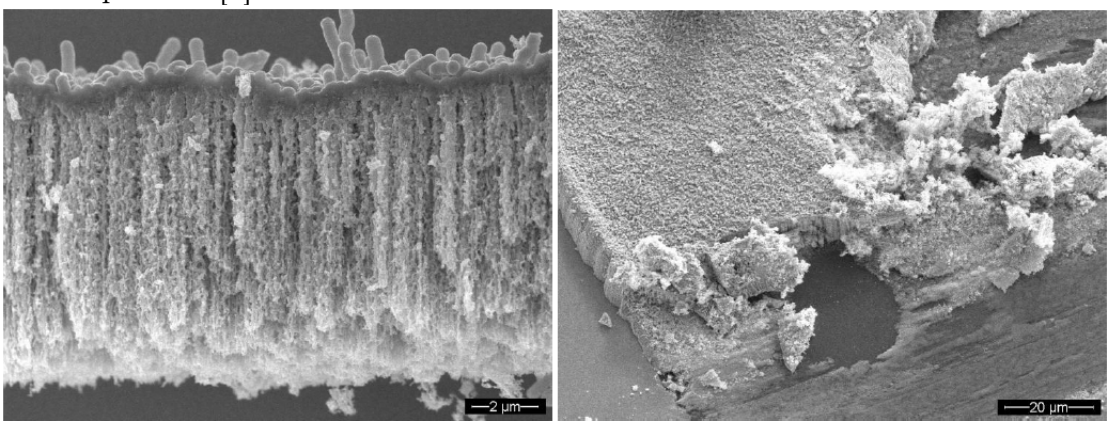

to be hot, and the walls of the chamber to be cold. Then most of the deposition will be on the substrate rather than the walls of the chamber. This reaction occurs at temperatures of 300 ºC and greater.

The main reason that we chose ALD as our deposition method was to solve the problem of uneven infiltration and cracking. Previous students at BYU studied the infiltration of CNT forests by metalorganic chemical vapor deposition (MOCVD), using the precursors tungsten carbonyl ($W(CO)_6$) and molybdenum carbonyl ($Mo(CO)_6$)[4]. They found that molybdenum was easier to use for infiltration and they found process parameters where efficient and even deposition could be achieved. For tungsten, the infiltration was never successful enough for testing (see fig 1.2), and thus we then endeavored to infiltrate using ALD.

Figure 1.5: Scanning micrograph of tungsten selectively deposited on patterned Si/SiO_2.[3]

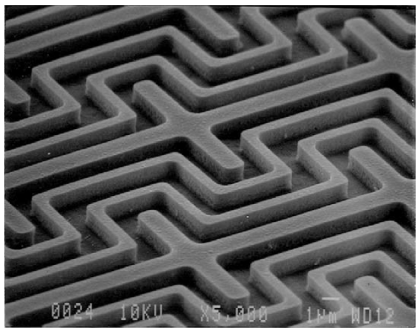

1.4 Selective Deposition of Tungsten

I will discuss later in the results section some of the difficulties regarding the tungsten ALD process. One method to help start a more even coating of the CNT forest is the selective deposition of tungsten on silicon.

$$2WF_{6\,(g)} + 3Si_{(s)} \Longrightarrow 2W_{(s)} + 3SiF_{4\,(g)} \tag{1.2}$$

In this reaction, the tungsten hexafluoride is reduced by elemental silicon. The silicon dioxide cannot reduce the tungsten molecule because it is already fully oxidized. In the example electron micrograph, the tungsten will not react with the silicon dioxide and selectively deposits on the elemental silicon, thus forming the pattern.

Chapter 2

Experimental Methods

2.1 CNT-M template and growth process

The CNT-M process has been adequately covered in previous literature and other undergraduate theses. Therefore I will only present a brief overview of the CNT-M process, with a diagram for good measure. A wafer is prepared by standard photolithographic processes, by which we get a patterned layer of iron on the wafer. This patterned sample is placed in a furnace at 750 ºC. Hydrogen and ethylene are flowed over the sample for 30 sec to 180 sec, depending on growth height desired. As the gases flow, carbon nanotube forests grow vertically up from the patterned iron. In this manner, I can produce a very specifically patterned CNT forest.

Figure 2.1: CNT-M method cross-section diagram. (a) 30 nm of Al_2O_3 is deposited on the substrate by E-beam evaporation. (b) Photoresist is then spun onto substrate and patterned by photolithography. (c) 6 nm of Fe is thermally evaporated onto the substrate. (d) Photoresist is then lifted off, leaving behind patterned Fe. (e) Fe serves as a catalyst for CNT growth by CVD. (f) Infiltration of metal by CVD or in this case, ALD. (g) CNT composite is released by etching underlying SiO_2 layer. [4]

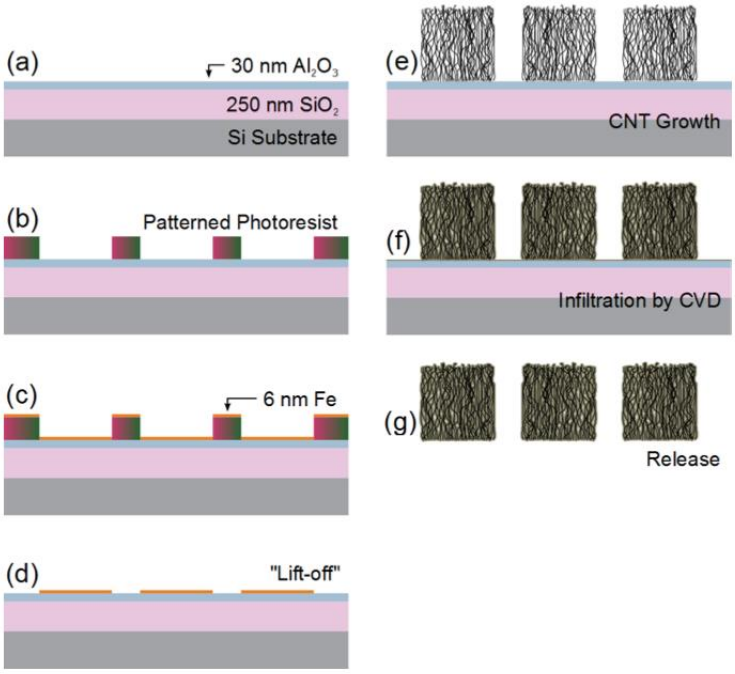

2.2 Modification of the system

Figure 2.2: Diagram of the System

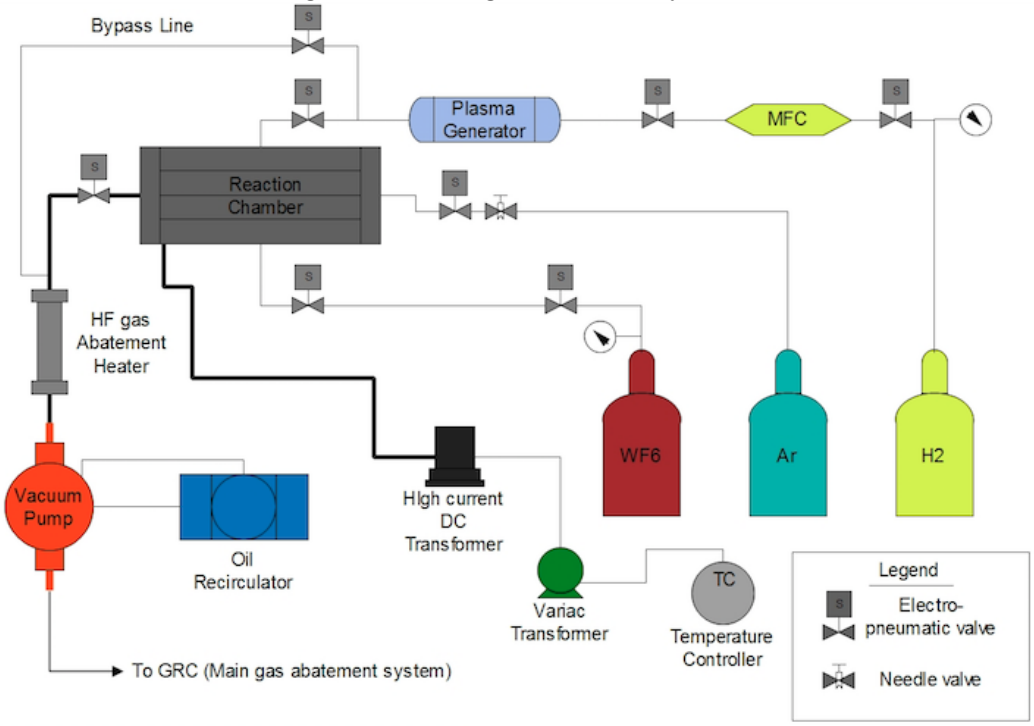

Figure 2.3: Labview Front Panel for ALD

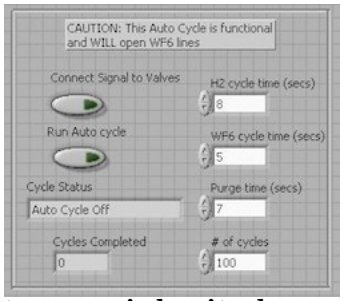

The system we inherited was a simple cold-wall chemical vapor deposition system built inside an old gas cabinet. My colleague and I had to connect the right valves and lines to the system, and plumb a sufficient exhaust line. The gas is carried through stainless steel lines and connected to the valves using VCR and some Swagelock connections. The source bottle

for the tungsten hexafluoride was mounted on the inside of the cabinet, and the cabinet then was exhausted in accordance with appropriate safety procedures. As explained in the chapter 1, the ALD reaction creates hydrogen fluoride as a byproduct, a very reactive and toxic gas. I made a small gas abatement system to react some of the hydrogen fluoride before it went to the pump. The reaction of the hydrogen fluoride with the pump oil proved to be a major issue, as one pump was rendered inoperable. To prevent the same fate befalling our second pump, I purchased and installed a recirculating oil filtration system to take care of the impurities in the pump oil. I also took advantage of an old temperature controller to provide the system with more accurate control of the substrate temperature. The temperature controller puts out 120 VAC to a variac for moderation, which then connects to a transformer. The transformer lowers the voltage and raises the current in order to be more efficient for our resistive heater. I connected and tuned a Opthos Instruments microwave plasma generator to form a hydrogen plasma from hydrogen gas right before entering the chamber.

Figure 2.4: State machine in Labview code

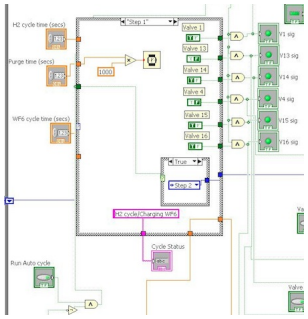

The most needed modification was an automated program for cycling the valves for the precursor and purge gases. The previous system had a Labview program for controlling the numerous valves. I added a state machine program to the Labview code that would automate the

valves with input for tungsten hexafluoride time, hydrogen time, purge time and number of cycles to complete. We used argon as the purge gas. Finally, I leak tested the system many times over the research project. This was imperative, since any oxygen in the system would give us tungsten oxide rather than the tungsten we wanted. We generally operated the system at a pressure of 1 torr with the purge gas running at about 50 standard cubic centimeters per min (sccm).

2.3 Ozone Treatment

One of the methods that I tried in order to get better infiltration of the CNT forest was to ozone treat the sample before placing the sample in the system. This involved placing the sample on a boat inside of a quartz tube. This was connected to a Absolute Ozone Titan 30 ozone generator. I flowed oxygen into the ozone generator and then over the sample at 1 standard cubic foot per hour (SCFH) for 20-25 min, and then placed the sample inside of the deposition chamber. In the future, we may be able to produce an oxygen plasma *in situ* to ozone treat our samples without exposing them to air before deposition.

2.4 SEM/XEDS Characterization

I characterized the samples using scanning electron microscopy (SEM) and X-ray electron dispersive spectroscopy (XEDS). I also gave some samples to a professor to be analyzed using transmission electron spectroscopy (TEM) so that I could get selected area diffraction images. Using these images, I could determine the lattice spacing of the crystals seen in SEM

Figure 2.5: SEM setup for concentration vs. depth scans

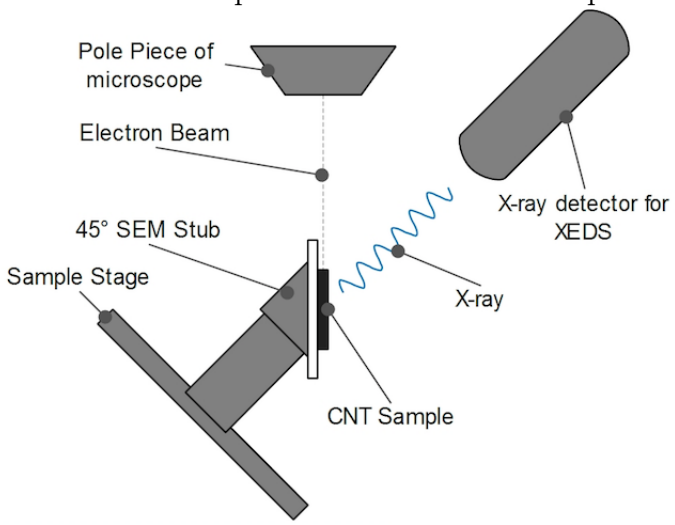

micrographs, and determine if the crystals were, in fact, tungsten. In the figure above, we have a diagram of the setup to determine tungsten concentration according to depth. We sourced some 45º SEM stubs from Ted Pella Inc so that we could orient our sample a total 90º from the incoming electron beam. We removed some of the CNT forest so that we could analyze a surface that was not exposed during deposition. Thus we now can use XEDS to determine the extent of infiltration vs depth in the forest.

2.5 Silicon Infiltration

I prepared a CNT sample that was partially infiltrated with silicon using CVD. During the course of this research, we did not have our usual method of silicon deposition by pyrolysis of silane in equation 2.1, so we tried the decomposition of dichlorosilane found in equation 2.2. This was because of the changing of silane tanks due to fire code restrictions. With the

dichlorosilane reaction, we also added hydrogen gas to attempt to force the reaction to the right of the equation.

$$SiH_{4\,(g)} \Longrightarrow Si_{(s)} + 2H_{2\,(g)} \tag{2.1}$$

$$SiCl_2H_{2\,(g)} \Longrightarrow Si_{(s)} + 2HCl_{(g)} \tag{2.2}$$

This process was done by flowing dichlorosilane gas over the sample at 800 ºC for 25 min. (SEM analysis of silicon infiltration)

Chapter 3

Results

Figure 3.1: Tungsten crystals on a CNT forest

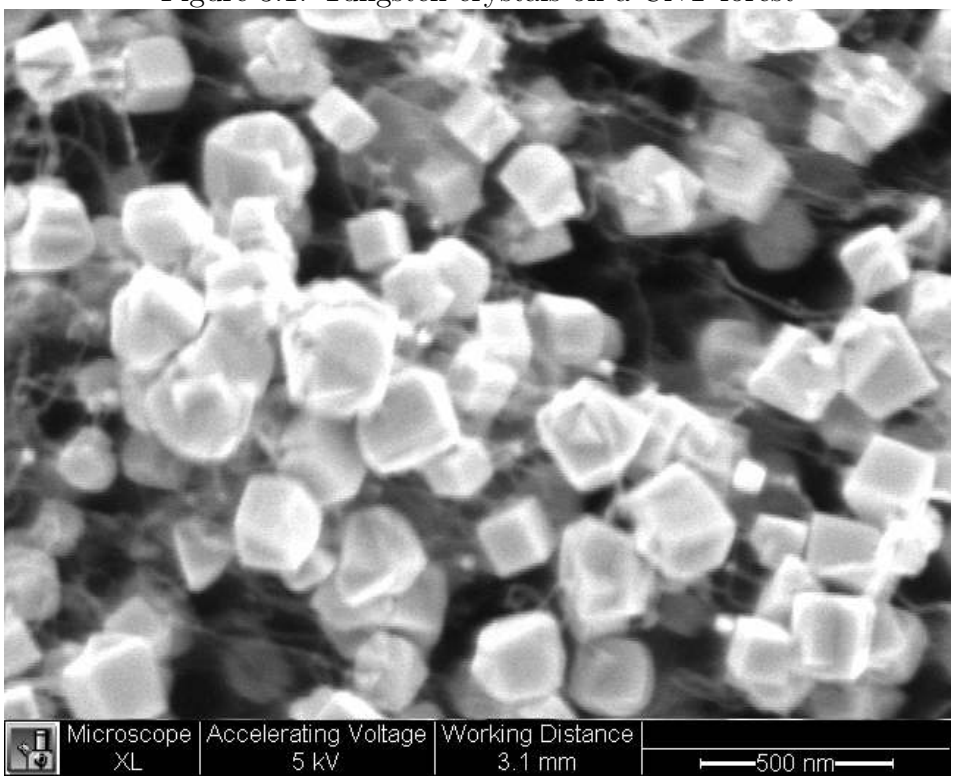

3.1 XEDS Results

In studying the XEDS data from each sample, we must be careful to notice that the sample is most often on a silicon substrate. The Kα X-ray line for silicon is at 1.74 eV, while the Mα X-ray line for tungsten is at 1.775 eV[13]. These two lines are really too close to accurately resolve with the XEDS module, and so some of the data pointing to tungsten will not be accurate. In order to better quantify the amount of tungsten in the sample, we used higher electron energies around 15 keV so we could see the Lα and other lines in tungsten around 8 eV. Also, the quantity data from the XEDS should be considered with the knowledge that none of these scan were done with a standard, and so the data is somewhat relative.

3.2 Ozone vs No Ozone

Figure 3.2: SEM/XEDS analysis of regular sample

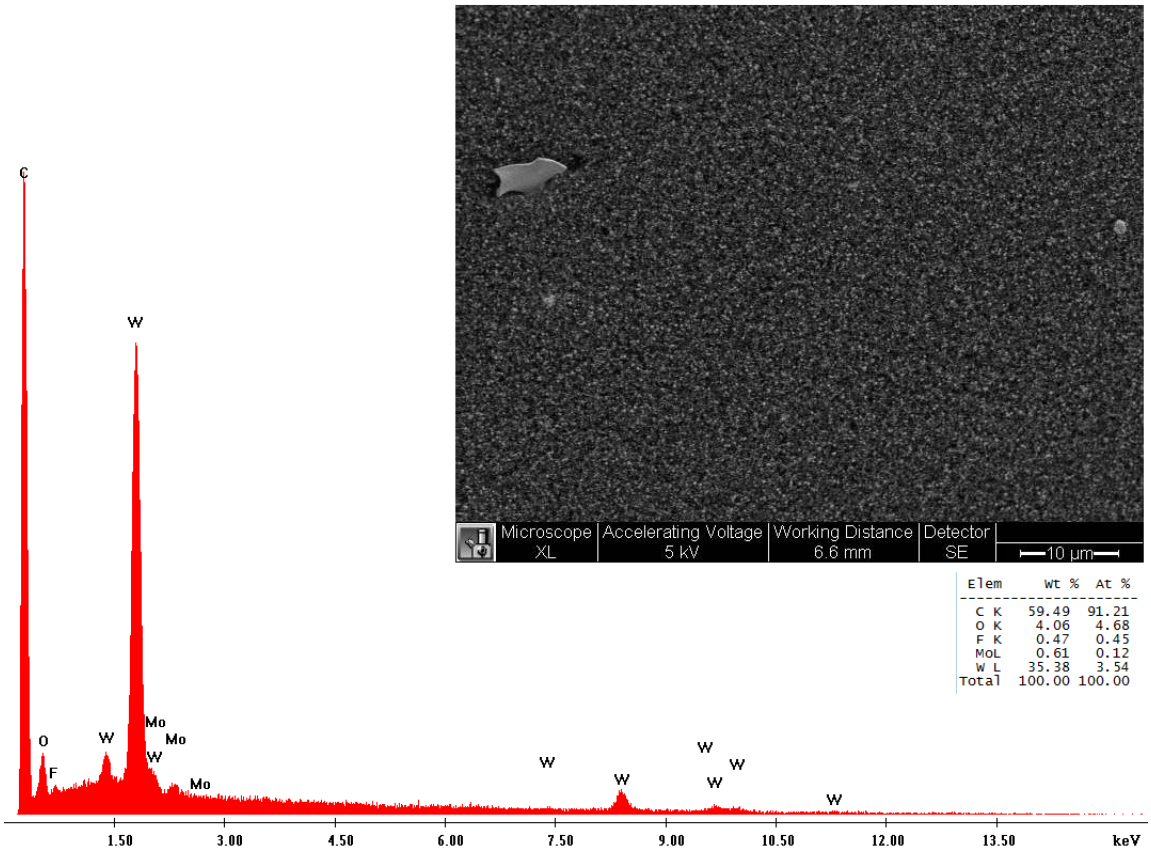

At the suggestion of one of my colleagues, I treated the CNT forest with ozone as described in Chapter 2. Based on visual inspection of the samples, SEM micrographs, and XEDS data, we can see that we had greater deposition with the ozone treatment than without for the same number of cycles. From the XEDS peaks we see a carbon peak on the none ozone treated sample, and much less of a carbon peak on the ozone treated sample. This can tell us that the relative amount of tungsten to carbon is much greater on the ozone treated sample compared to the other sample.

Figure 3.3: SEM/XEDS analysis of ozone treated sample

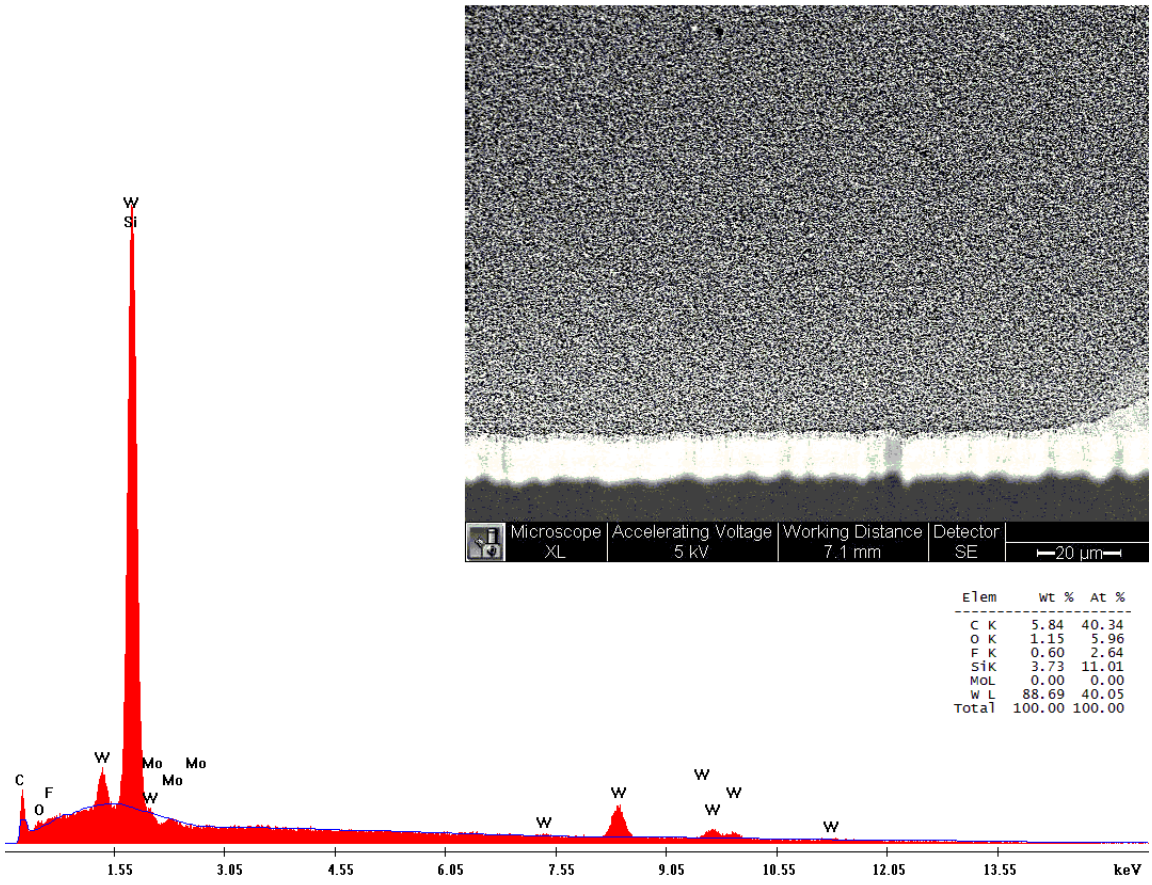

Since the carbon content of both samples is very similar, we can tell that there is much more tungsten on the ozone treated sample. Based on this information, most of the samples created after I had done this experiment were treated with ozone before deposition.

3.3 Plasma

Using a hydrogen plasma to get hydrogen radicals instead of molecular hydrogen was another suggestion for better deposition. Using a hydrogen plasma did give us better deposition for the same number for cycles, but

Figure 3.4: SEM/XEDS of regular deposition

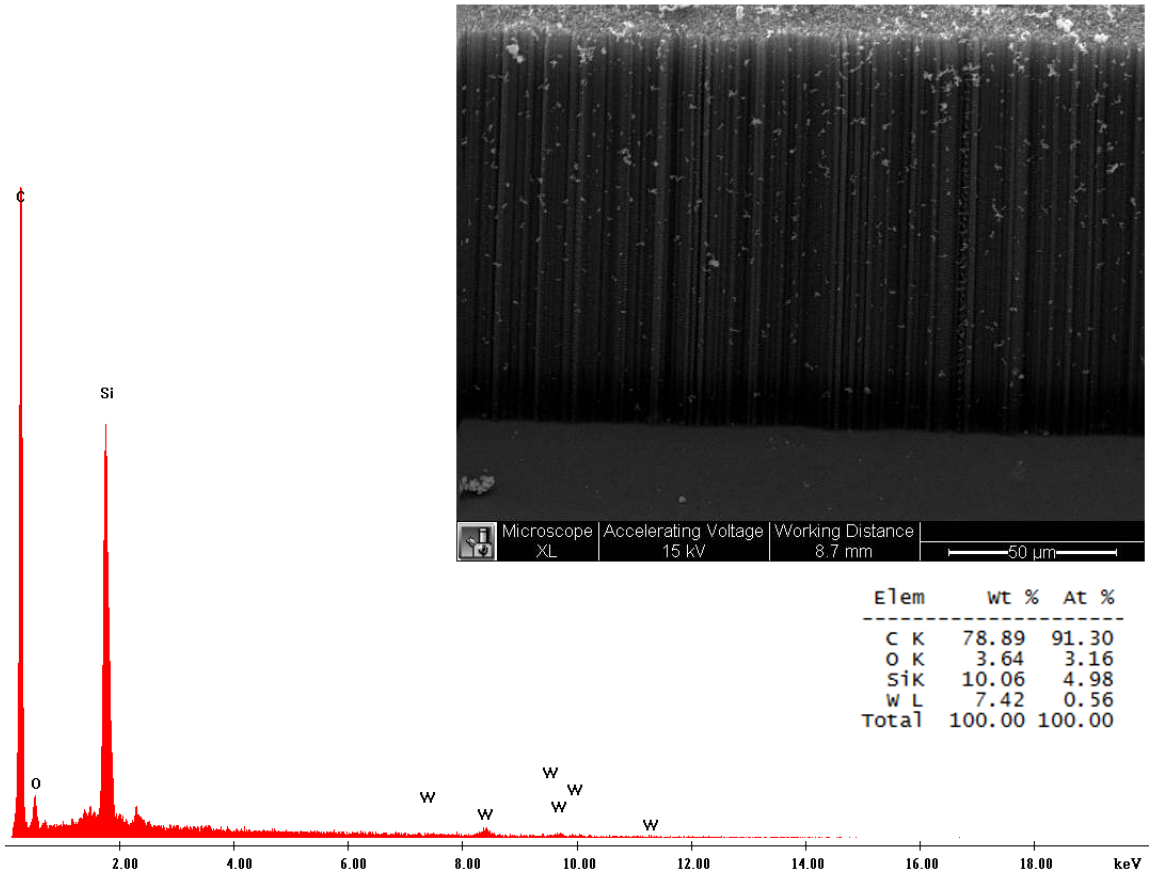

did not give us better infiltration into the CNT forest. Almost all of the good samples that we have were done with both ozone treatment and plasma. Due to time constraints, we do not have good results for infiltration with only ozone treatment and no plasma treatment at lower temperatures.

Figure 3.5: SEM/XEDS of deposition with plasma

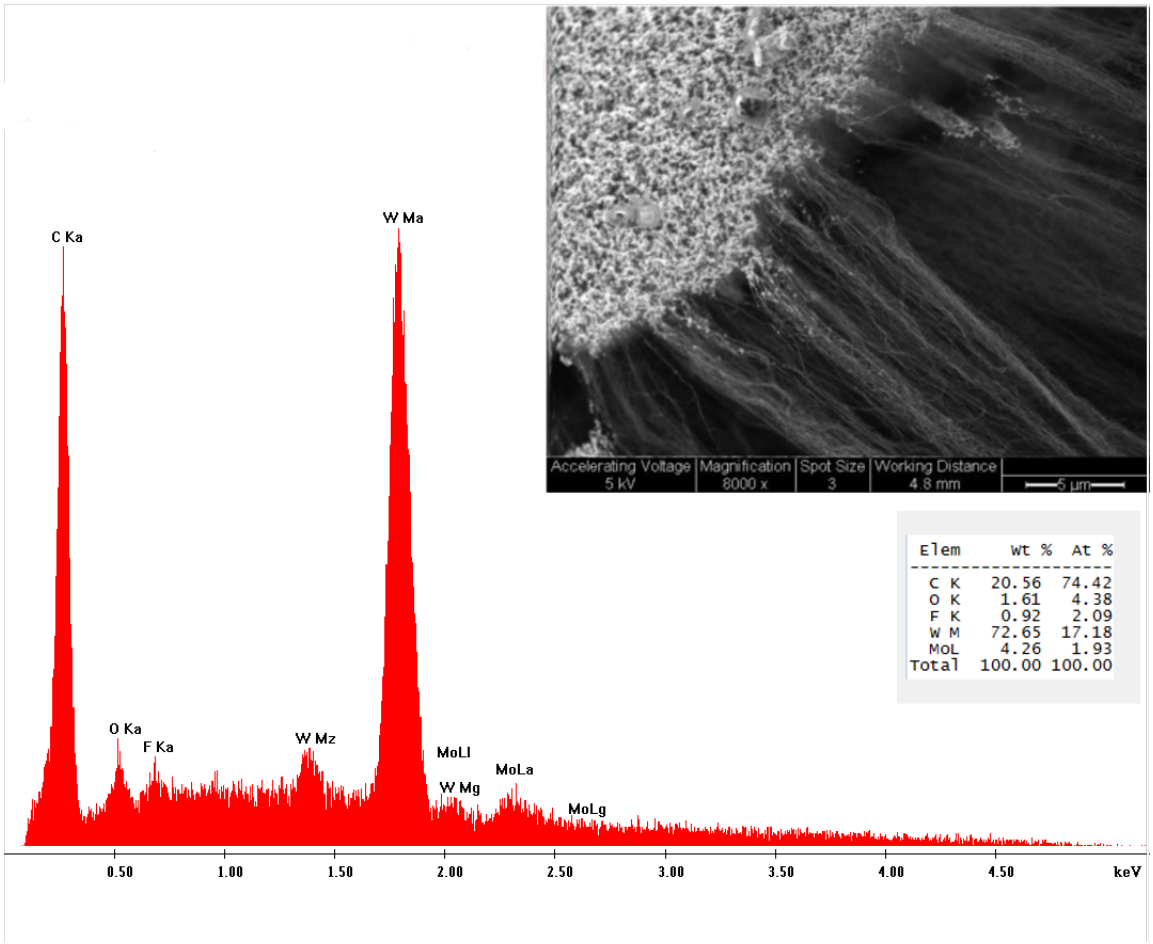

3.4 Tungsten concentration vs depth

Figure 3.6: Line scan of a tungsten infiltrated sample

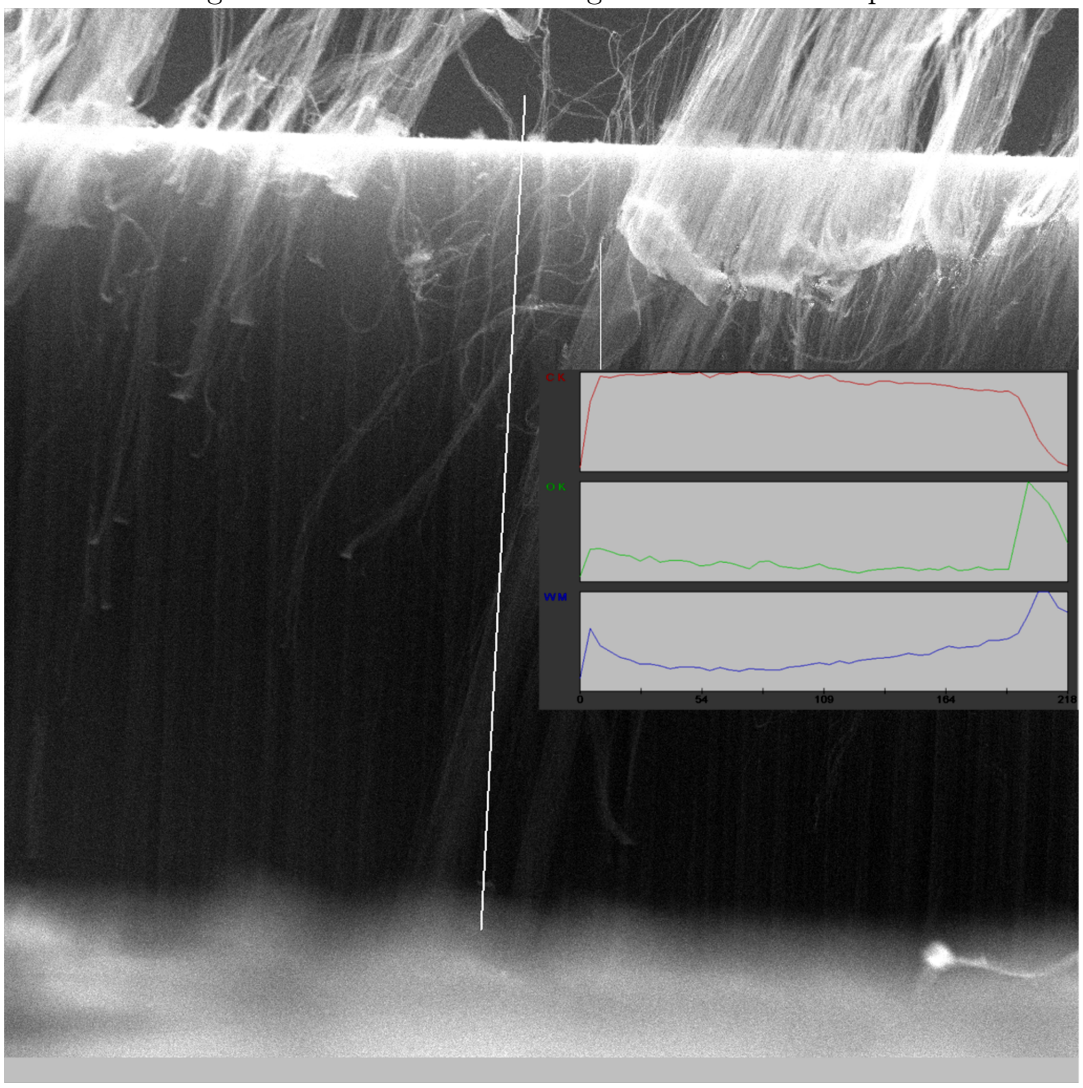

As described in section 2.4, I analyzed one of our later samples to see the concentration of the tungsten metal compared with the depth in the forest. I first separated part of the forest so that I was analyzing a part of the forest that was internal during deposition. As expected, the concentration drops off as depth increases until the very bottom of the forest. This increase at the bottom may be due to deposition on the substrate and not in the

actual CNT forest.

3.5 Infiltration by silicon replacement

At the time of submission of this paper, I have not been able to successfully make any silicon infiltrated forests in order to test the silicon replacement process. This is partially a result from the remodeling of the lab and attempting to adhere to correct fire code procedures. Therefore, there will be no discussion of results pertaining to silicon replacement.

Chapter 4

Discussion of Results

4.1 Ozone vs No Ozone

As described in Chapter 1, carbon nanotubes are formed from strong sp_2 hybridized bonds. We hypothesized that the tungsten was having a hard time breaking into those bonds in order to deposit. The suggestion to ozone treat the samples came from the idea that the ozone would break some of the sp_2 bonds and give more sites for tungsten nucleation. As seen in chapter 3, we did get more deposition on the ozone treated samples, especially on the exposed sides and top of the CNT forest. Whatever mechanism prevents the tungsten from infiltrating deep into the forest, the same mechanism may prevent the infiltration of ozone, and thus the breaking of bonds deep in the forest to a lesser extent. This would be one explanation for the small amount of tungsten deposition seen in the CNT samples.

4.2 Plasma

From the diagram of the system in chapter 2, we can see that the plasma is a remote plasma, and not actually in the deposition chamber as it is in plasma enhanced deposition methods (PECVD, PEALD). This means that there is definitely some recombination of the radicals back to molecular hydrogen before reaching the sample. Since our temperatures have been in the range needed for the regular reduction of tungsten hexafluoride by hydrogen, it is difficult to know how much this plasma is really helping. Further studies with plasma should be done in temperatures lower than 300 ºC, where the reduction by molecular hydrogen is unlikely. Modifiying the system so that the plasma is close to the substrate would help us better understand if atomic hydrogen can reduce tungsten hexafluoride effectively.

4.3 Conclusion

$$\lambda_{mfp} P = 5 * 10^{-5} \text{ torr·cm} \tag{4.1}$$

From chapter 2, we see that the deposition occurs at about 1 Torr. Using equation 4.1, we get the mean free path of the general molecule to be about 0.5 μm. This mean free path was thought to be enough to get some distance into the nanotube forest, but maybe not all the way to the bottom. Most sample forests that were used were from 100 to 400 μm. However, we never saw great deposition throughout the forest, and we did see a gradient from the top to the bottom as seen in the line scan in section 3.4. Thus, another option to try besides plasma, ozone, silane and

Figure 4.1: W ALD film thickness vs cycle number

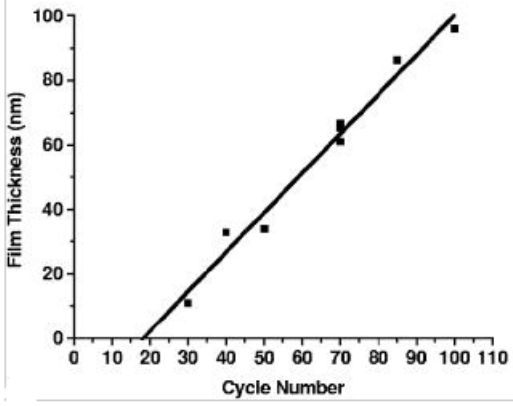

[14]

varying the substrate temperature would be to lower the pressure. This could allow the necessary molecules to penetrate farther into the nanotube forest. Again using equation 4.1, if we want the mean free path to be 500 μm, then the pressure of the deposition chamber must at or below 1 mTorr. This would require a different vacuum system then the current setup, as the base pressure now only reaches 400 mTorr. For a deposition, we would need a system with a base pressure in the μTorr range, and one that could withstand the corrosive HF gas that is produced.

The mean free path is not only important with regard to the height of the nanotube forest, but also to the space available in and between the nanotubes. A WF_6 molecule is about 6-7 angstroms or .6-.7 nm[15]. The average diameter of a carbon nanotube can vary, but we can assume that the diameter is 15 nm for our case. Thus, with our mean free path of 0.5 μm, the WF_6 molecule will bounce or stick a number of times before reaching the bottom of the forest. We can see that the infiltration into the forest is not just a function of forest height or nanotube diameter.

We should also consider the number of cycles when investigating the amount of infiltration in the carbon nanotube samples. From the theory of tungsten ALD in chapter 1, we know that each cycle should deposit only 1 layer of tungsten atoms. The paper on tungsten ALD by Lei tells us that each layer is only a couple of nanometers[14]. Also graph. Most of our depositions were between 60-100 cycles. From Lei's paper, we see that we would have deposited 40-80 nm of tungsten on a flat surface. Since carbon nanotube forests are 99 percent void, they have incredible surface area. Therefore 40-80 nm deposited throughout the forest may not be very much. In order to get a fairly solid tungsten structure, we may need to run many, many more cycles.

Since this project was in some ways cut short by various factors, it will be up to the next student researcher to study the effects of pressure, number of cycles, silicon infiltration and reduction by silane. Hopefully this paper can help the next researcher understand and learn how to create MEMS from tungsten and other refractory metals.

Bibliography

[1] "What is MEMS Technology,", 2014.

[2] Arnero, "Carbon nanotube armchair povray,".

[3] M. Ohring, *Material Science of Thin Films*, 2 ed. (Elselvier, 2002).

[4] R. Hansen, "Mechanical And Electrical Properties of Carbon-Nanotube-Templated Metallic Microstructures," Honors thesis, published by Brigham Young University Honors Department (2012).

[5] STMicroelectronics, "MEMS and Sensors,", 2014.

[6] J. Yeom, Y. Wu, J. C. Selby, and M. A. Shannon, "Maximum achievable aspect ratio in deep reactive ion etching of silicon due to aspect ratio dependent transport and the microloading effect," Journal of Vacuum Science & Technology B **23,** 2319–2329 (2005).

[7] S. Iijima, "Helical microtubules of graphitic carbon," Nature **7,** 354 (1991).

[8] L. Zhang, X. Tu, K. Welsher, X. Wang, M. Zheng, and H. Dai, "Optical Characterizations and Electronic Devices of Nearly Pure (10,5) Single-Walled Carbon Nanotubes," Journal of the American Chemical Society **131,** 2454–2455 (2009).

[9] E. Pop, D. Mann, Q. Wang, K. Goodson, and H. Dai, "Thermal Conductance of an Individual Single-Wall Carbon Nanotube above Room Temperature," Nano Letters **6,** 96–100 (2006).

[10] M.-F. Yu, O. Lourie, M. J. Dyer, K. Moloni, T. F. Kelly, and R. S. Ruoff, "Strength and Breaking Mechanism of Multiwalled Carbon Nanotubes Under Tensile Load," Science **287,** 637–640 (2000).

[11] D. N. Hutchison, "Vertically Aligned Carbon Nanotubes as a Framework for Microfabrication of High Aspect Ratio MEMS," Undergraduate thesis, published by Brigham Young University Department of Physics and Astronomy (2008).

[12] T. S. Wood, "Mechanical Properties of a-Carbon Infiltrated Carbon Nanotube Templated Materials," Honors thesis, published by Brigham Young University Honors Department (2011).

[13] "EDAX Periodic Table of Elements,", 2014.

[14] W. Lei, "Real-time observation and optimization of tungsten atomic layer deposition process cycle," J. Vac. Sci. Technol. B 24 (2006).

[15] T. Saito, Y. Shimogaki, Y. Egashira, K. Sugawara, K. Takahiro, S. Nagata, S. Yamaguchi, and H. Komiyama, "Kinetic study of chemical vapor deposition of {WSix} films from {WF6} and SiH2Cl2: Determination of molecular size and reactivity of gas species," Thin Solid Films **513,** 36 – 42 (2006).

[16] D. N. Hutchison, "Carbon nanotubes as a framework for high aspect ratio MEMS fabrication," J. MEMS **19,** 75–82 (2010).

[17] C. R. Kleijn, *Modeling of Chemical Vapor Deposition of Tungsten Films* (Birkhauser Verlag Basel, 1993).

[18] T. T. Kodas, *The Chemistry of Metal CVD* (John Wiley and Sons, 2008).

[19] D. M. McKenna, "Tungsten Infiltrated Carbon Nanotube Forests As A Framework for 3-D Microfabrication," Undergraduate thesis, published by Brigham Young University Department of Physics and Astronomy (2011).

[20] J. E. J. Schmitz, *Chemical Vapor Deposition of Tungsten and Tungsten Silicides* (Noyes Publications, 1992).

[21] J. Song, D. S. Jensen, D. N. Hutchison, B. Turner, T. Wood, A. Dadson, M. A. Vail, M. R. Linford, R. R. Vanfleet, and R. C. Davis, "Carbon-Nanotube-Templated Microfabrication of Porous Silicon-Carbon Materials with Application to Chemical Separations," Advanced Functional Materials **21,** 1132–1139 (2011).